Microscopic Model for High-spin vs. Low-spin ground state in [Ni2M(CN)8](M=MoV, WV, NbIV) magnetic clusters

Rajamani Raghunathan, Jean-Pascal Sutter, Laurent Ducasse, Cédric Desplanches, S. Ramasesha

Microscopic model for high-spin versus low-spin ground state in $[Ni_2M(CN)_8](M=Mo^V,W^V,Nb^{IV})$ magnetic clusters

Rajamani Raghunathan,[1,*] Jean-Pascal Sutter,[2,†] Laurent Ducasse,[3,‡] Cédric Desplanches,[4,§] and S. Ramasesha[1,‖]
[1]*Solid State and Structural Chemistry Unit, Indian Institute of Science, Bangalore 560 012, India*
[2]*Laboratorie de Chimie de Coordination du CNRS, Université Paul Sabatier, 205, Route de Narbonne, 31077 Toulouse, France*
[3]*Laboratoire de Physico-Chimie Moléculaire, UMR 5803 du CNRS, Université Bordeaux I, 351 Cours de la Libération, 33405 Talence, France*
[4]*Institut de Chimie de la Matiére Condensée de Bordeaux, CNRS, 87 Avenue Dr. Schweitzer, F-33608 PESSAC, France*
(Received 24 November 2005; revised manuscript received 21 February 2006; published 24 March 2006)

Conventional superexchange rules predict ferromagnetic exchange interaction between Ni(II) and $M(M=Mo^V, W^V, Nb^{IV})$. Recent experiments show that in some systems this superexchange is antiferromagnetic. To understand this feature, in this paper we develop a microscopic model for Ni(II)-*M* systems and solve it exactly using a valence bond approach. We identify the direct exchange coupling, the splitting of the magnetic orbitals and the interorbital electron repulsions, on the *M* site as the parameters which control the ground state spin of various clusters of the Ni(II)-*M* system. We present quantum phase diagrams which delineate the high-spin and low-spin ground states in the parameter space. We fit the spin gap to a spin Hamiltonian and extract the effective exchange constant within the experimentally observed range, for reasonable parameter values. We also find a region in the parameter space where an intermediate spin state is the ground state. These results indicate that the spin spectrum of the microscopic model cannot be reproduced by a simple Heisenberg exchange Hamiltonian.

DOI: 10.1103/PhysRevB.73.104438 PACS number(s): 75.50.Xx, 71.27.+a, 75.30.Et, 75.40.Mg

I. INTRODUCTION

In the expanding field of molecular magnetism, transition metal complexes have been the main focus of study. Room temperature bulk magnetization has been achieved with a hybrid organic radical/V(II) framework[1] and also with the Cr(III)/V(II) Prussian blue type compound.[2,3] Besides, interesting conjectures such as the Haldane conjecture[4] have been verified in molecular systems.[5] The interest in molecular magnetism has expanded in recent times to include low-dimensional architectures exhibiting slow relaxation of magnetization known as single molecule magnets (SMMs),[6] conducting magnets,[7] and light-triggered magnets.[8] The large majority of these molecular compounds are based on paramagnetic 3*d* metal ions, and the second and third row transition metal ions have been envisaged only recently for the construction of magnetic supramolecular compounds.[9] These ions appear however very promising in molecular magnetism yielding magnets with fairly high ordering temperatures,[10] new SMM's,[11] and efficient systems with light triggered magnetization changes.[12] The 4*d* and 5*d* ions are characterized by spatially more extended valence orbitals, the extension following the trend $3d<4d<5d$. A consequence of this ordering of the *d*-orbital is that the on-site electron repulsion is decreased as we go down the column in the Periodic Table. Besides, the metal-ligand bonds become more covalent resulting in more efficient electron delocalization. A series of experimental results obtained on simple cyano-bridged heterometallic species formed by self-assembling of an octacyanometallate ($\{Mo^V(CN)_8\}^{3-}$ or $\{W^V(CN)_8\}^{3-}$) with a $\{Ni^{II}L\}^{+2}$ complex (*L*= macrocyclic ligand) showed that the nature of the effective superexchange through the cyano-bridge depends upon the actual spin topology of the complex that is being studied. For instance, whereas significant ferromagnetic interactions are found for linear {Ni-*M*-Ni} compounds ($M=Mo^V$ or W^V in the $[\{M(CN)_8\}]$ unit), an antiferromagnetic behavior is observed for a cyclic tetranuclear compound (Fig. 1).[13] A related larger spin clusters of formula $[\{NiL\}_{12}\{Nb(CN)_8\}_6]$ exhibits an even more complex magnetic behavior.[14]

In this paper, we explain this puzzling nature of the superexchange interaction between two transition metal ions *A* and *B*, each containing two nearly degenerate orbitals, by developing a microscopic model which naturally admits antiferromagnetic exchange interactions between them. The ion *A* has two electrons while *B* has one electron; these correspond to the case of Ni^{II} for the *A* ion and either Mo^V, W^V or Nb^{IV} for the *B* ion. The parameters entering the definition of the microscopic model are the on-site and intersite parameters. The on-site parameters are both one and two-electron parameters. The one-electron parameters are energy differences between the active magnetic orbitals on *A* and *B*, and the splitting of the two orbitals on *B*.[15] The two electron parameters are the electrostatic on-site Hubbard repulsion terms and the interorbital Coulomb and exchange integrals. The intersite one-electron parameters are the transfer integrals and the intersite two-electron Coulomb interactions in the zero differential overlap approximation. We identify the critical interaction parameters that control the sign of the superexchange interaction and present a quantum phase diagram that shows a crossover in the ground state from effective ferromagnetic interaction to effective antiferromagnetic interaction between the ions. We show this behavior in different organizations of the *AB* system such as *A*-*B*, linear

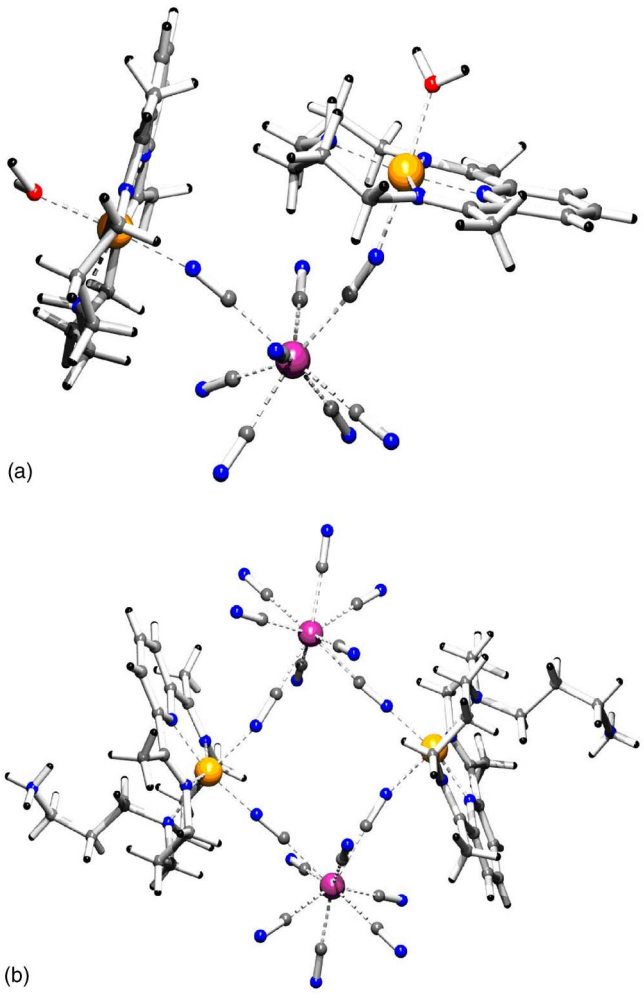

FIG. 1. (Color online) Views of the supramolecular compounds top: $[\{NiL\}_2\{M(CN)_8\}]^+$ and bottom: $[\{NiL'\}_2\{M(CN)_8\}_2]$.

A-B-A, *B-A-B*, *A-B-A-B*, and cyclic *A-B-A-B* clusters. In Sec. II we introduce the microscopic model for superexchange in the $Ni^{II}_{S=1}$-$M^{V}_{S=1/2}$ system. This is followed by Sec. III in which we describe the valence bond (VB) method for solving the model. Section IV deals with the results and their discussion.

II. MODEL HAMILTONIAN FOR SUPEREXCHANGE IN *AB* SYSTEMS

The nature of exchange interaction between two ions is the outcome of a competition between delocalization of the electrons which reduces the kinetic energy and direct exchange interactions which reduces the electron-electron repulsion energy for parallel spin alignment. Usually, the kinetic energy is decreased if the electrons are in a low-spin state; in the high spin state, the delocalization of electrons is blocked because of the Pauli exclusion. Besides, low-spin configuration also usually affords more phase space for electron delocalization. This is why the kinetic exchange is usually antiferromagnetic in nature. However, when there is a near degeneracy of the partially occupied orbitals on an ion, then delocalization is possible even when the spins are aligned parallel and indeed, the direct exchange interaction favors parallel electron spin alignment on such degenerate sites. In this case, the final outcome cannot be easily predicted and depends upon the actual values of the interaction parameters. Thus, a microscopic model for explaining the observed sign of the exchange interaction should include direct exchange interactions between nearly degenerate orbitals on a given site and the relative splitting of the degenerate orbitals. Besides these terms, another interaction term of considerable importance is the strength of the intraorbital electron repulsions relative to the strength of on-site interorbital electron repulsions. This is because, if the interorbital intrasite electron repulsions is weak compared to the intraorbital electron repulsion, it will favor single occupancy of two orbitals on the same site over double occupancy of one of the orbitals. Occupancy of the orbitals controls the nature of the superexchange process, thus the relative strengths of on-site inter- and intraorbital repulsions become very important. The other interaction terms which are comparable in strength to these repulsion integrals are the intersite electron-electron interactions within the zero differential overlap approximation and the intrasite electron repulsion between a charge density in one orbital and a charge density in the overlap cloud of two orbitals, which we call the *W* term. The model Hamiltonian for investigating the superexchange interaction can be written as

$$\begin{aligned}\hat{H} = & \sum_i \epsilon_i \hat{n}_i + \sum_{\langle ij \rangle} t_{ij}(\hat{E}_{ij} + \hat{E}_{ji}) + \sum_i \frac{U_i}{2}\hat{n}_i(\hat{n}_i - 1) \\ & + \sum_{i,i'} \Bigg\{ U_{i,i'}\hat{n}_i\hat{n}_{i'} + \frac{W_{i,i'}}{2}\Bigg[(E_{i,i'} + E_{i',i})(\hat{n}_i + \hat{n}_{i'}) \\ & + (\hat{n}_i + \hat{n}_{i'})(E_{i,i'} + E_{i',i}) - 2((E_{i,i'} + E_{i',i})\Bigg] \\ & + \frac{J_{i,i'}}{2}(E_{i,i'}E_{i,i'} + E_{i',i}E_{i',i} + E_{i,i'}E_{i',i} + E_{i',i}E_{i,i'} - \hat{n}_i - \hat{n}_{i'}) \Bigg\} \\ & + \sum_{\langle ij \rangle} \frac{V_{ij}}{2}\hat{n}_i\hat{n}_j,\end{aligned}$$

$$\hat{n}_i = \sum_\sigma a^\dagger_{i,\sigma}a_{i,\sigma}, \quad \hat{E}_{i,j} = \sum_\sigma a^\dagger_{i,\sigma}a_{j,\sigma}, \tag{1}$$

where, the summation runs over all the orbitals and operator $a^\dagger_{i,\sigma}$ ($a_{i,\sigma}$) creates (annihilates) an electron in orbital i with spin σ. The first line corresponds to the noninteracting part of the Hamiltonian with ϵ_i being the energy of the ith orbital, and t the transfer integral between an orbital on one site and another on the neighboring site. All values of t are assumed to be the same and the orbital energy of the *A*-type atoms are fixed at zero, while the orbital energies of the *B*-type atoms are $-\Delta$ and $(-\Delta + \delta_B)$ as shown in Fig. 2. The third term corresponds to the intraorbital interaction term, with U_i being the Hubbard parameter. The remaining lines except the last represent the interorbital on-site electron repulsion terms, $U_{i,i'} = [ii|i'i'] = \int\int \phi_i^*(1)\phi_i(1)\frac{1}{r_{12}}\phi_{i'}^*(2)\phi_{i'}(2)d^3r_1 d^3r_2$, $W_{ii'} = [ii|ii'] = \int\int \phi_i^*(1)\phi_i(1)\frac{1}{r_{12}}\phi_i^*(2)\phi_{i'}(2)d^3r_1 d^3r_2$, and $J_{ii'}$

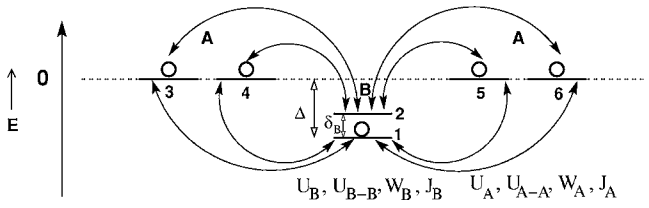

FIG. 2. Schematic diagram of the active orbitals and the interactions in the *A-B-A* system. The transfer terms included in the model are shown by filled double-headed arrows between pairs of orbitals. Since, only two orbitals are considered on each site, the interaction terms are labeled by the site indices (A/B).

$=[ii'|ii']=\int\int \phi_i^*(1)\phi_{i'}(1)\frac{1}{r_{12}}\phi_i^*(2)\phi_{i'}(2)d^3r_1d^3r_2$, where $J_{ii'}$ is the exchange integral. These integrals are assumed to be nonzero only when orbitals i and i' are on the same site (or ion). Since we deal with only two types of ions A and B, and only two orbitals on each ion, we label these as U_A, $U_{A\text{-}A}$, W_A, and J_A for the A ions and similarly for the B ions. The last line corresponds to the intersite interorbital repulsion integral $V_{ij}=[ii|jj]=\int\int \phi_i^*(1)\phi_i(1)\frac{1}{r_{12}}\phi_j^*(2)\phi_j(2)d^3r_1d^3r_2$ and is parametrized using Ohno parametrization[16] and appropriate scaling.[17]

The magnitude of the intra-atomic electron repulsion integrals are in the order $U_A > U_{A\text{-}A} > W_A > J_A$; $U_B > U_{B\text{-}B} > W_B > J_B$. For isolated atoms, these parameters can be determined from experimental energies of various spectral terms and using Condon-Shotkey or Racaah expressions for the term energies. These parameters can also be determined theoretically using the approach of Gunnarsson.[18,19] In case of solids, particularly the high-T_c oxide superconductors these interaction parameters for the transition metal ions have been determined from photoemission studies.[20,21]

III. SOLUTION OF THE SUPEREXCHANGE MODEL

The Hamiltonian in Eq. (1) is nonrelativistic and hence conserves total spin. Since we are interested in the solution of the model in different total spin sectors, we use the valence bond technique for solving the model. In this technique, the complete and linearly independent basis states with a given total spin can be generated using explicit spin pairings.[22] For example, if singly occupied sites i and j are spin paired, then a line is drawn between sites i and j in the VB diagram to indicate the spin pairing, $(\alpha_i\beta_j-\beta_i\alpha_j)/\sqrt{2}$, $i<j$. We say that the line begins at site i and ends at site j. If the spins at sites $i_1, i_2, \ldots, i_l$ are not paired, we pass an arrow through these sites in the VB diagram and this denotes the state $\alpha_{i_1}\alpha_{i_2}\cdots\alpha_{i_l}$. Because the Hamiltonian conserves S^z_{total} besides S^2, it is sufficient to work in the subspace $M_S=S$. In the $S=0$ subspace, a VB diagram has either empty and doubly occupied sites (represented by dots and crosses, respectively) or lines between singlet paired singly occupied sites. A VB diagram involving N orbitals can be drawn by arranging the orbitals at the vertices of a regular N-gon and drawing straight lines between vertices, the electrons at whose orbitals are singlet paired. The Rumer-Pauling rule states that all such VB diagrams with no intersecting lines form a complete and linearly independent set.[23] The complete and linearly independent set of VB states in nonzero spin space can be obtained by taking recourse to the modified Rumer-Pauling rules.[22] Each orbital in the VB picture has one of four possibilities: (i) the orbital is empty, (ii) the orbital is doubly occupied, (iii) a line begins at the orbital, or (iv) a line ends at the orbital. It is possible to associate these four possibilities of an orbital in a VB diagram with the four states of two bits in an integer, identified with the orbital.[22] Thus, for an eight orbital system, the VB diagrams are represented by a sixteen bit integer and these integers can be generated in an ascending order. In any given spin space, the effect of the operator term $\hat{E}_{ij}$ in the Hamiltonian on a basis state is to alter the orbital occupancy of orbitals i and j (subject to Pauli principle) and pair the spins in the orbitals that were involved to yield a new VB diagram with a known amplitude. If the new VB diagram violates Rumer-Pauling rules, it is trivially possible to express it as a linear combination of the basis VB states.

Using the above procedure, the Hamiltonian matrix can be set-up in the chosen total spin sector. The resulting Hamiltonian matrix is sparse (since the number of terms in the Hamiltonian is far smaller than the dimension of the complete VB space) and nonsymmetric and can be partially diagonalized to obtain a few of the low-lying eigenstates, using Rettrup's modification of the Davidson algorithm, when the Hilbert space dimensionality is large.[24,25] In our case, since the dimensionalities of the different subspaces are fairly small (the largest subspace encountered is of dimensionality 1512 for the $S=1$ subspace in the *A-B-A-B* system), full diagonalization of the Hamiltonian matrix is resorted to in each spin sector to obtain the complete eigenvalue spectrum.

IV. RESULTS AND DISCUSSION

The range of values of on-site electron repulsion integrals take is known for the transition metal ions and it is reasonable to assume that U_A, when A represents Ni^{2+} is smaller than U_B when B corresponds to M (Mo^V,W^V,Nb^{IV}), since the higher charge on the M ion should make the orbitals more compact, resulting in larger intraorbital electron repulsion integrals. It is reasonable to assume U_A to be 6 eV and U_B to be 8 eV. Indeed, we have also verified that the results we present do not change qualitatively when these parameters are allowed to vary by up to 2 eV about the mean values. The parameters $U_{A\text{-}A}$ and $U_{B\text{-}B}$ are slightly smaller than the corresponding intraorbital repulsion integral. The integrals W_A and W_B are much smaller than the $U_{A\text{-}A}$ or the $U_{B\text{-}B}$ integrals as they involve overlap charge densities and both W_A and W_B have been fixed at 1 eV. The exchange integrals J_A and J_B are somewhat smaller than the integrals W_A and W_B. We also note that since it is experimentally known that the spin on the A ion (Ni^{2+}) is always one we fix J_A at a somewhat large value of 0.7 eV. Large J_A reduces the repulsion between electrons with parallel spin alignment compared to antiparallel spin alignment in the two orbitals on site A leading to a spin-1 object on site A and this holds

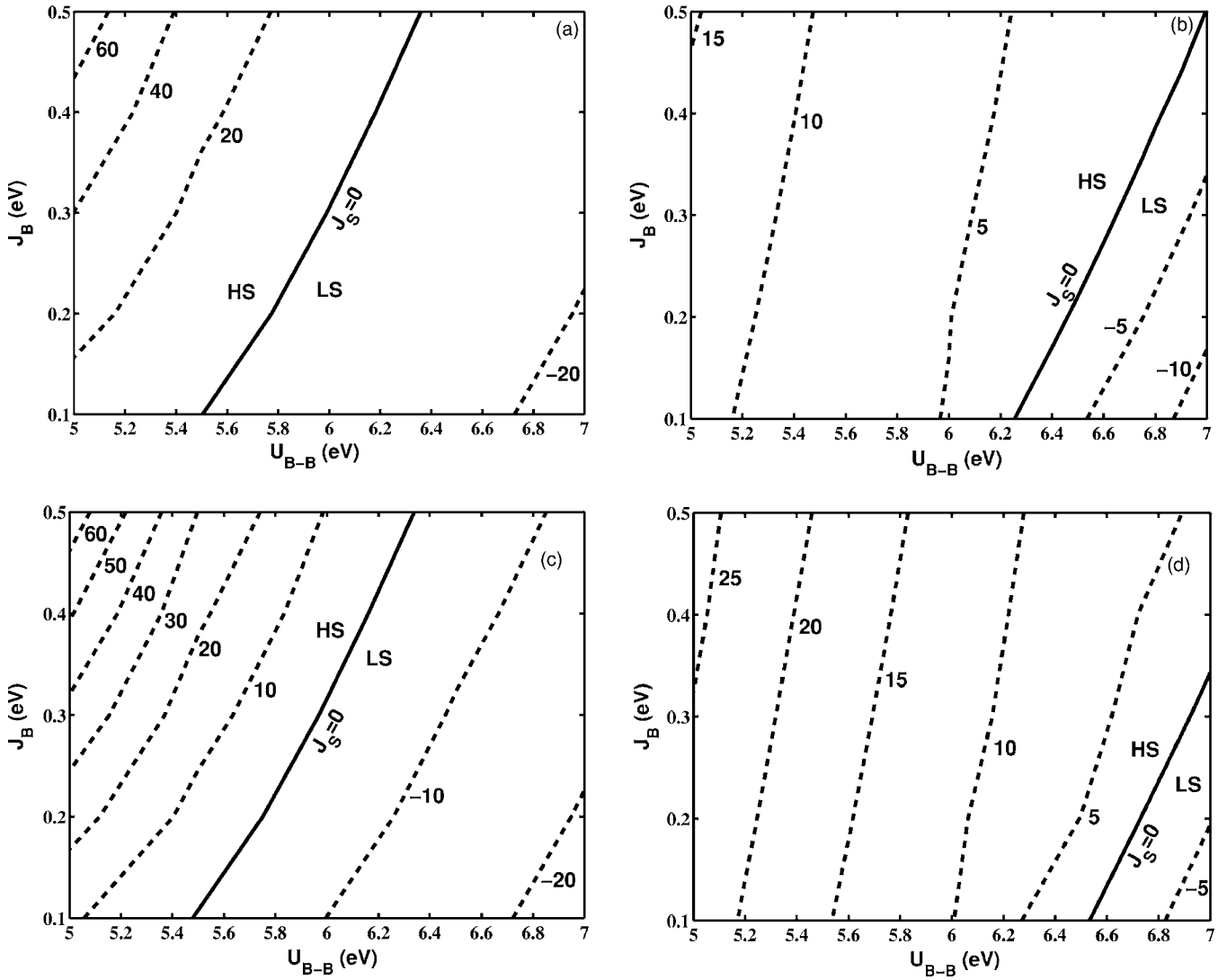

FIG. 3. Contours of the effective superexchange constants (J_S cm^{-1}) of (a) *A-B*, (b) *A-B-A*, (c) *B-A-B* chains, and (d) cyclic *A-B-A-B* systems as a function of $U_{B\text{-}B}$ and J_B. The phase diagrams are obtained for t=0.1 eV, Δ=0.0 eV; δ_B=0.0 eV; U_A=6 eV; U_B=8 eV; $U_{A\text{-}A}$=4 eV; J_A=0.7 eV; W_A=W_B=1 eV. All the systems display high-spin ground state at higher J_B and lower $U_{B\text{-}B}$ values.

true even when the degeneracy of the two orbitals on the *A* site is slightly lifted. For this reason, we have assumed the two orbitals on *A* to be degenerate. In each case, we have also verified that the expectation value of $\hat{S}_A^2$ operator is nearly 2.0 confirming that the spin on the *A* site is very nearly one in all cases. The total spin of the system in the ground state is sensitive to the parameters δ_B, J_B, and $U_{B\text{-}B}$. A large δ_B would result in an antiferromagnetic exchange interaction since the virtual state with a doubly occupied lower orbital on the *B* site has a lower energy than the spin one state on the *B* ion. A large J_B would however lower the energy of the virtual state in which the *B* ion has a spin one configuration. A small $U_{B\text{-}B}$ would also favor a spin one virtual state on the *B* ion by favoring single occupancy of the two active *B* ion orbitals. We have solved the model Hamiltonian over a wide range of parameters and have obtained the quantum phase diagrams for demarcating the low-spin and high-spin ground states in this parameter space.

At each point in the parameter space, we obtain the difference in energy, ΔE, between the lowest states of the model Hamiltonian in the high-spin and low-spin sectors. We fit ΔE to the spin Hamiltonian H_S=$J_S\Sigma_{nn}S_A\cdot S_B$ (the summation is over nearest neighbors of the *A-B* system) to determine the effective superexchange parameter, J_S. In Figs. 3–5 we have presented the contours of superexchange values (J_S) in these systems for various values of the model parameters. The solid line corresponding to J_S=0 provides the phase boundary between the high-spin and low-spin ground states. The contours corresponding to fixed J_S values and represented by dotted lines are obtained by spline interpolation using MATLAB. We note that small $U_{B\text{-}B}$, small δ_B and large J_B values promote a high spin ground state while large $U_{B\text{-}B}$, large δ_B and small J_B values promote a low spin ground state. We also note that the superexchange J_S values, for the same model parameters, are larger for smaller system sizes.

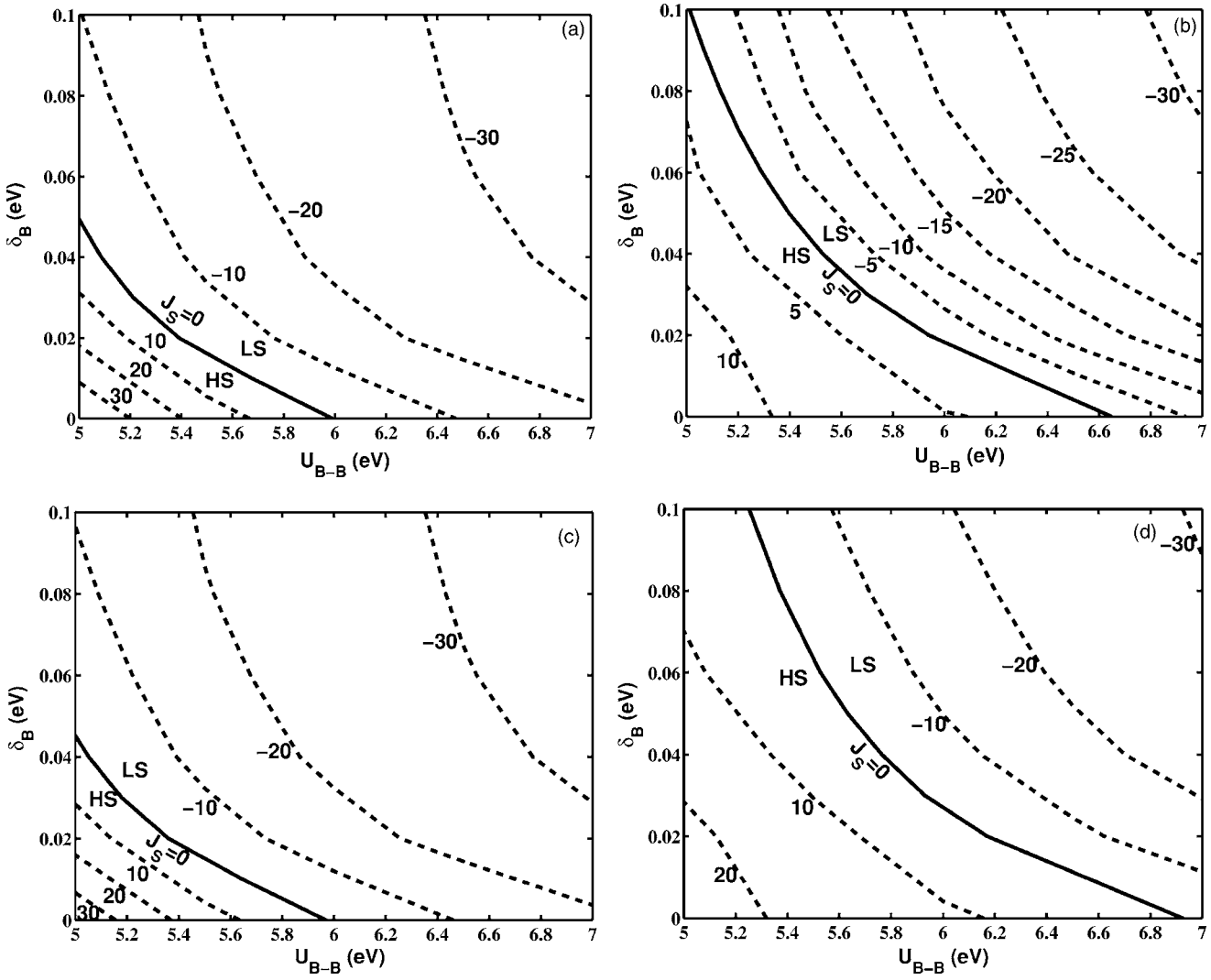

FIG. 4. Contours of the effective superexchange constants (J_S cm^{-1}) of (a) *A-B*, (b) *A-B-A*, (c) *B-A-B* chains, and (d) cyclic *A-B-A-B* systems as a function of δ_B and $U_{B\text{-}B}$. The phase diagrams are obtained for t=0.1 eV, Δ=0.0 eV; U_A=6 eV; U_B=8 eV; $U_{A\text{-}A}$=4 eV; J_A=0.7 eV; J_B=0.3 eV; W_A=W_B=1 eV. All the systems display high-spin ground state at lower δ_B and $U_{B\text{-}B}$ values.

A. Phase diagram in the $U_{B\text{-}B}$-J_B plane

In the $U_{B\text{-}B}$-J_B plane, we should expect to see the high-spin ground state for large J_B and small $U_{B\text{-}B}$. This is because the large exchange integral on the *B* site will favor parallel alignment of the electrons on the *B* site, if the virtual transfer of the electron does not lead to a doubly occupied *B* site orbital. The latter requirement is guaranteed if $U_{B\text{-}B}$ is small. In Fig. 3 we see that in all the cases, the ground state corresponds to the high spin state for small $U_{B\text{-}B}$ and large J_B. We also note from the shift in the phase line to the right, that with increase in system size the high-spin state is favored for larger $U_{B\text{-}B}$ values. From the gap between the high spin and the low spin states, we have also calculated the effective superexchange parameter. We find that the largest ferromagnetic superexchange J_S value is 101.42 K (70.49 cm^{-1}) for $U_{B\text{-}B}$=5 eV and J_B=0.5 eV, while the largest antiferromagnetic superexchange J_S value corresponds to −33.36 K (−23.19 cm^{-1}) for $U_{B\text{-}B}$=7 eV and J_B=0.1 eV in the linear *A-B* cluster. Another interesting feature to note is that in the *B-A-B* cluster, the low-spin ground state appears for a much smaller $U_{B\text{-}B}$ value, for a given J_B than in the *A-B-A* cluster.

B. Phase diagram in the $U_{B\text{-}B}$-δ_B plane

The phase diagram in the $U_{B\text{-}B}$-δ_B plane for all the four systems is shown in Fig. 4. We note that the ground state spin is extremely sensitive to the δ_B value. Even a small splitting of the *B* site orbitals forces the system into a low-spin ground state. This is because the lifting of the degeneracy of the *B* site orbital favors doubly occupied lower energy orbitals in the virtual state, which would result in stabilization of the low-spin state. Here again, we note that the high spin ground state is more robust in the larger clusters. In the cyclic *A-B-A-B* cluster, for $U_{B\text{-}B}$=5.5 eV, the ground state shifts to low-spin state for δ_B=0.063 eV while in the *A-B-A* cluster, this occurs at δ_B=0.04 eV and in the

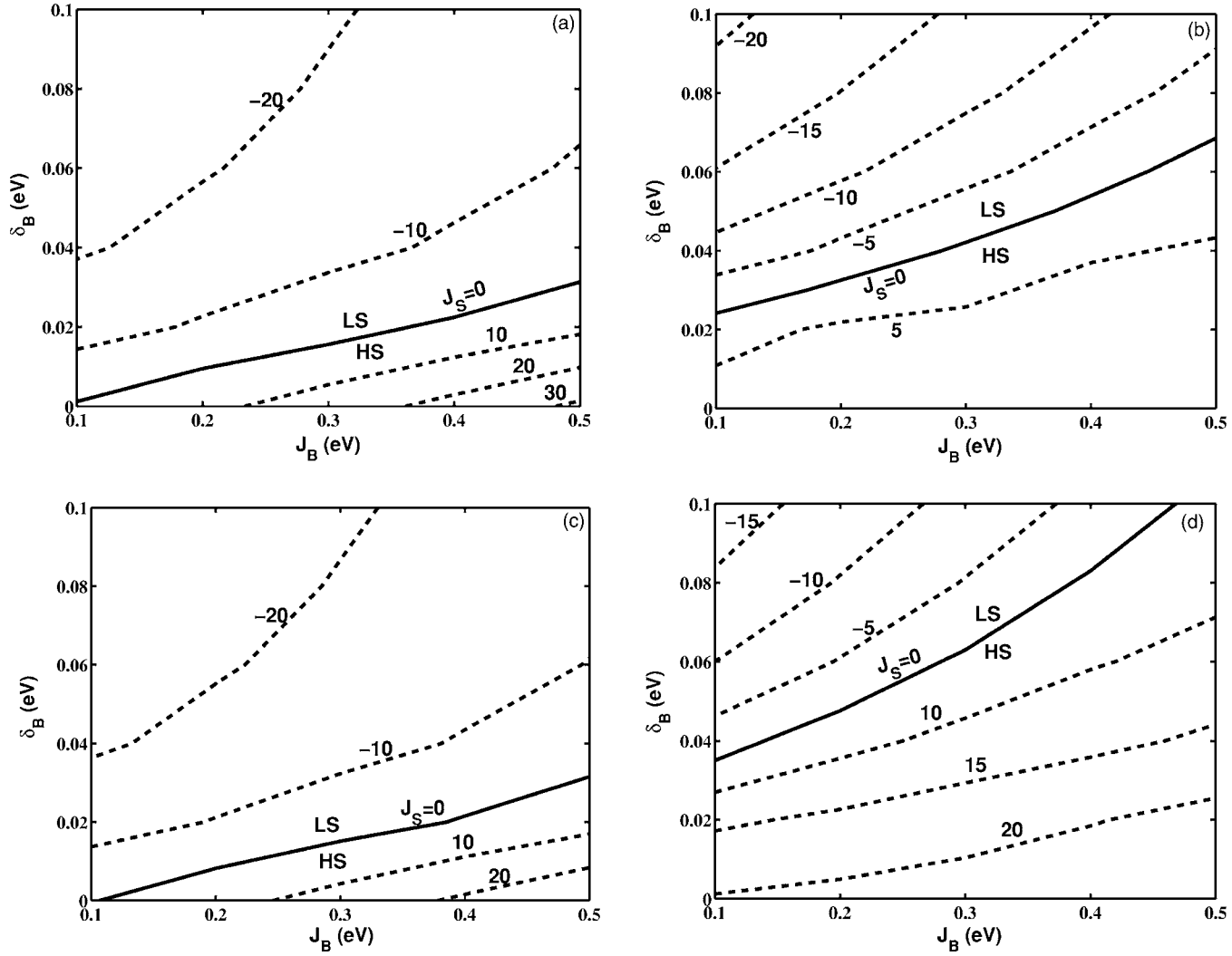

FIG. 5. Contours of the effective superexchange constants (J_S cm^{-1}) of (a) *A-B*, (b) *A-B-A*, (c) *B-A-B* chains, and (d) cyclic *A-B-A-B* systems as a function of J_B and δ_B. The phase diagrams are obtained for t=0.1 eV, Δ=0.0 eV; U_A=6 eV; U_B=8 eV; $U_{A\text{-}A}$=4 eV; $U_{B\text{-}B}$=5.5 eV; J_A=0.7 eV; W_A=W_B=1 eV. All the systems display high-spin ground state at lower δ_B and higher J_B values.

A-B system the ground state ceases to be the high spin state for $\delta_B > 0.016$ eV. The highest ferromagnetic superexchange constant J_S is observed for δ_B=0 and $U_{B\text{-}B}$=5 eV while the highest antiferromagnetic J is observed for δ_B=0.1 eV and $U_{B\text{-}B}$=7 eV in all the clusters. We also can note that for a given δ_B value, we have a low spin ground state in the *B-A-B* system, at much smaller value of $U_{B\text{-}B}$ value than in the *A-B-A* system.

C. Phase diagram in the J_B-δ_B plane

Large values of δ_B has the effect of promoting the antiferromagnetic superexchange while a large J_B favors ferromagnetic superexchange. Thus, we see from Fig. 5 that the high spin state is the ground state below the phase line while the low-spin state is the ground state above the phase line. The phase line shifts higher in the J_B-δ_B plane as the system size is increased thereby showing that the high spin ground state is more stable to lifting of the degeneracy of the orbitals on the *B* site for larger system sizes. In this plane, the behavior of the *A-B-A* and the *B-A-B* systems are almost identical.

Our studies, besides identifying the critical parameters that determine the ground state spin also show the dependence of the spin in the ground state on the system size. The high-spin state is stabilized relative to the low-spin state to a greater extent in the larger system, as is seen from the larger region covered by the high-spin state in the *A-B-A-B* cyclic system in the phase diagrams in all the three planes. Experimentally, however, the cyclic *A-B-A-B* is in a low spin ground state. This implies that the parameters in the cyclic *A-B-A-B* system is not the same as in the other systems. It is likely that the degeneracy of the orbitals on the *B* site is lifted more in the cyclic *A-B-A-B* system than in the chains due to ring strains.

One very interesting feature not clearly seen in the phase diagrams of the cyclic *A-B-A-B* cluster is the appearance of the intermediate spin S=2 ground state over a very narrow

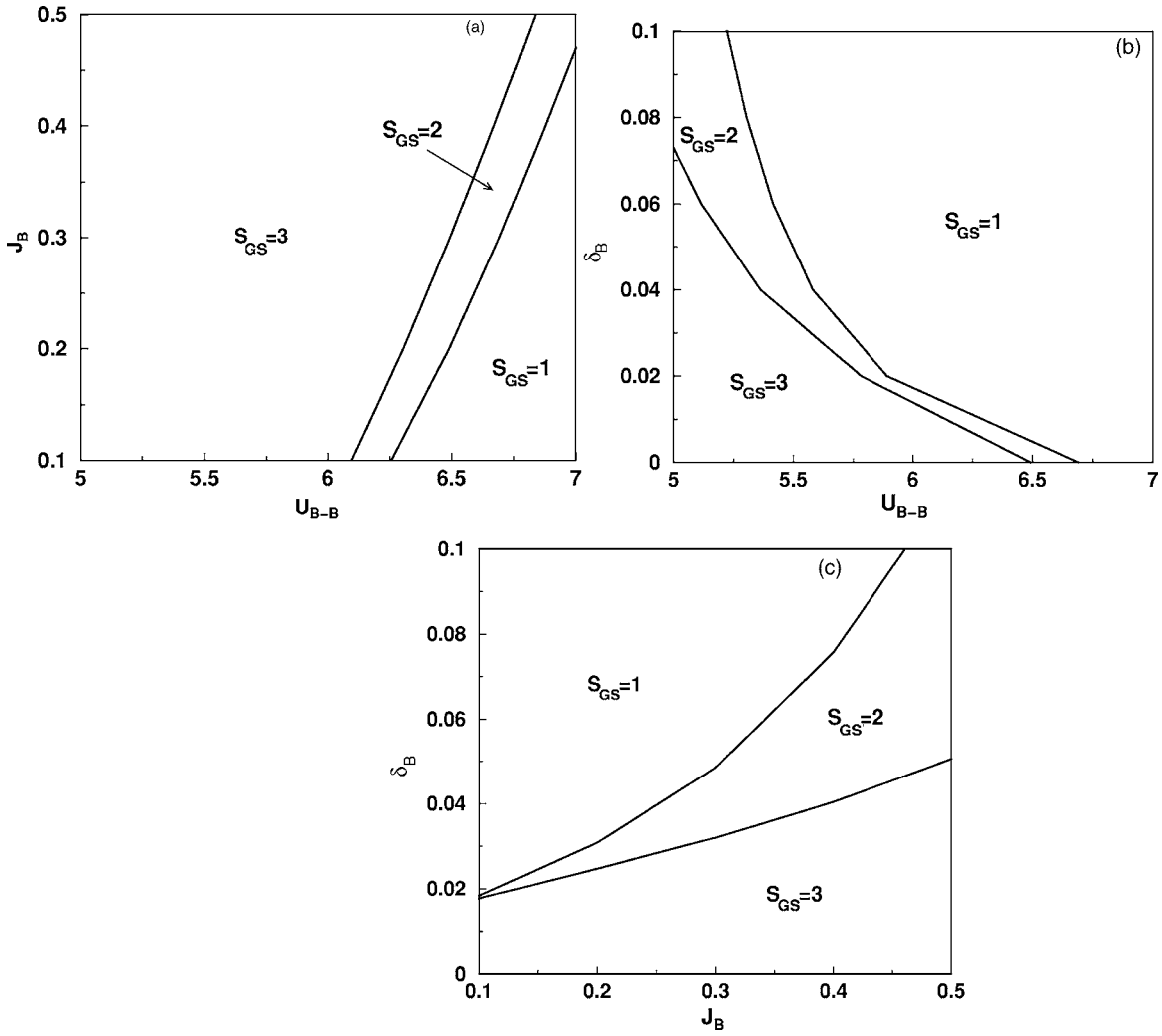

FIG. 6. Phase diagrams of linear *A-B-A-B* system in (a) $U_{B\text{-}B}$-J_B (b) $U_{B\text{-}B}$-δ_B, and (c) J_B-δ_B planes. S_{GS} is the ground state spin of the system. It is interesting to see the appearance of intermediate spin ground state $S_{GS}=2$ for a wide range of parameter values, which is not prominent in the cyclic *A-B-A-B* system.

range of parameter values between the $S=1$ and the $S=3$ ground states. The intermediate spin ground state is seen only in the largest cluster we have studied. In fact, in the linear *A-B-A-B* cluster, this region extends over a wider parameter values, as seen in Fig. 6. Thus, it may be possible to synthesize high nuclearity complexes in intermediate spin ground states. The physics behind the existence of such ground states is however somewhat different from the frustrated magnetic exchanges present in SMMs. In our case, it is difficult to identify the exchange interaction between two sites as either ferro or antiferromagnetic and magnetism can be viewed as a whole and not pairwise, as is usually the case. Besides, it is also not possible to map our model onto a simple Heisenberg exchange Hamiltonian.

To conclude, we have developed a model Hamiltonian which admits both low-spin and high-spin ground states for small changes in the values of the model parameters. The only model parameter that can perhaps be determined directly for a system is δ_B, from spectroscopic data. Other parameters can be inferred from electron spectroscopic studies and *ab initio* calculations on simple systems.[18,19] However, our quantum phase diagrams are quite robust to changes in the interaction parameters U_A, $U_{A\text{-}A}$, and U_B over a range of 2 eV. This range is expected to reasonably cover a wide range of chemical environments. Our model can explain the observed antiferromagnetic exchange in the Nb_6Ni_{12} and related systems, contrary to superexchange rules.[13,14] The model also yields reasonable effective superexchange constants for model parameters in the accepted range.

ACKNOWLEDGMENTS

The authors thank DST for the support received under a joint Indo-French Laboratory for Solid State Chemistry (IFLaSC) and Indo-French Centre for Promotion of Advanced Research (IFCPAR)/Centre Franco-Indien pour la Promotion de la Recherche Avancée (CEFIPRA) for generous support under Project No. 3108-3 on Design, Synthesis, and Modeling Molecular Magnets.

*Electronic address: rajamani@sscu.iisc.ernet.in
†Electronic address: sutter@lcc-toulouse.fr
‡Electronic address: l.ducasse@lpcm.u-bordeaux1.fr
§Electronic address: desplan@icmcb-bordeaux.cnrs.fr
‖Electronic address: ramasesh@sscu.iisc.ernet.in

[1] J. M. Manriquez, G. T. Yee, R. S. McLean, A. J. Epstein, and J. S. Miller, Science **252**, 1415 (1991).
[2] S. Ferlay, T. Mallah, R. Ouahés, P. Veillet, and M. Verdaguer, Nature (London) **378**, 701 (1995).
[3] S. M. Holmes and G. S. Girolami, J. Am. Chem. Soc. **121**, 5593 (1999).
[4] F. D. M. Haldane, Phys. Lett. **93A**, 464 (1983); , Phys. Rev. Lett. **50**, 1153 (1983).
[5] J. P. Renard, M. Verdaguer, L. P. Regnault, W. A. C. Erkelens, J. Rossat-Mignod, J. Ribas, W. G. Stirling, and C. Vettier, J. Appl. Phys. **63**, 3538 (1988).
[6] D. Gatteschi and R. Sessoli, Angew. Chem., Int. Ed. **42**, 269 (2003).
[7] E. Coronado, J. R. Galan-Mascaros, C. J. Gomez-Garcia, and V. Laukhin, Nature (London) **408**, 447 (2000).
[8] O. Sato, T. Iyoda, A. Fujishima, and K. Hashimoto, Science **272**, 704 (1996); V. Escax, A. Bleuzen, C. Cartier dit Moulin, F. Villain, A. Goujon, F. Varret, and M. Verdaguer, J. Am. Chem. Soc. **123**, 12536 (2001).
[9] C. Mathoniére, J.-P. Sutter, and J. V. Yakhmi, in *Magnetism: Molecules to Materials*, edited by J. S. Miller and M. Drillon (Wiley-VCH, Weinheim, 2002), Vol. 4, pp. 1–40, and references therein.
[10] S. Tanase, F. Tuna, P. Guionneau, T. Maris, G. Rombaut, C. Mathoniére, M. Andruh, O. Kahn, and J.- P. Sutter, Inorg. Chem. **42**, 1625 (2003).
[11] Y. Song, P. Zhang, X.-M. Ren, X.-F. Shen, Y.-Z. Li, and X.-Z. You, J. Am. Chem. Soc. **127**, 3708 (2005).
[12] J. M. Herrera, V. Marvaud, M. Verdaguer, J. Marrot, M. Kalisz, and C. Mathoniere, Angew. Chem., Int. Ed. **43**, 5468 (2004).
[13] J. -P. Sutter *et al.* (unpublished results).
[14] R. Pradhan, C. Desplanches, P. Guionneau, and J. P. Sutter, Inorg. Chem. **42**, 6607 (2003).
[15] The splitting of the degenerate orbitals on *A* is expected to be small as the *A* ion is always in the spin-1 state and the direct exchange integral involving these orbitals on *A* is large enough to ensure that such splitting does not result in spin pairing on the *A* site.
[16] K. Ohno, Theor. Chim. Acta **2**, 219 (1964); G. Klopmann, J. Am. Chem. Soc. **86**, 4450 (1964).
[17] M. Chandross, S. Mazumdar, M. Liess, P. A. Lane, Z. V. Vardeny, M. Hamaguchi, and K. Yoshino, Phys. Rev. B **55**, 1486 (1997).
[18] V. I. Anisimov and O. Gunnarsson, Phys. Rev. B **43**, 7570 (1991).
[19] O. Gunnarsson, Phys. Rev. B **41**, 514 (1990).
[20] A. Fujimori, Phys. Rev. B **28**, 4489 (1983).
[21] S. R. Barman and D. D. Sarma, Phys. Rev. B **49**(19), 13979 (1994).
[22] S. Ramasesha and Z. G. Soos, in *Valence Bond Theory*, edited by David L. Cooper (Elsevier Science, Amsterdam, 2002), Chap. 20, 635.
[23] G. Rumer, Nachr. Chem., Tech. Lab. 377 (1932).
[24] E. R. Davidson, J. Comput. Phys. **17**, 87 (1975).
[25] S. Rettrup, J. Comput. Phys. **45**, 100 (1982).